Journal of Catalysis 272 (2010) 18–27

Contents lists available at ScienceDirect

Journal of Catalysis

journal homepage: www.elsevier.com/locate/jcat

Mössbauer spectroscopy investigation and hydrodesulfurization properties of iron–nickel phosphide catalysts

Amy F. Gaudette [a,c], Autumn W. Burns [a,c], John R. Hayes [a,c], Mica C. Smith [a,c], Richard H. Bowker [a,c], Takele Seda [b,c], Mark E. Bussell [a,c,*]

[a] Department of Chemistry, MS-9150, Western Washington University, Bellingham, WA 98225, United States
[b] Department of Physics, MS-9164, Western Washington University, Bellingham, WA 98225, United States
[c] Advanced Materials Science and Engineering Center, Western Washington University, Bellingham, WA 98225, United States

ARTICLE INFO

Article history:
Received 9 February 2010
Revised 18 March 2010
Accepted 22 March 2010
Available online 18 April 2010

Keywords:
Hydrodesulfurization
HDS
Mössbauer spectroscopy
Nickel phosphide
Bimetallic phosphide
Iron–nickel phosphide

ABSTRACT

Unsupported and silica-supported $Fe_xNi_{2-x}P_y$ catalysts having a range of metal compositions ($0 < x \leqslant 2.0$) were investigated using Mössbauer spectroscopy, and the results correlated with the surface and hydrodesulfurization (HDS) properties of the supported catalysts. Mössbauer spectroscopy permits determination of the relative site occupancy of Fe atoms in tetrahedral (M(1)) and pyramidal (M(2)) sites in the $Fe_xNi_{2-x}P_y$ materials. Fe atoms preferentially occupy M(2) sites for materials with significant Fe contents ($x > \sim 0.60$), but the Fe site preference reverses as the Fe content decreases ($x < \sim 0.60$). Similar occupation trends are observed for the unsupported and silica-supported $Fe_xNi_{2-x}P_y$ materials. Thiophene HDS measurements of the $Fe_xNi_{2-x}P_y/SiO_2$ catalysts revealed catalysts with high Fe contents ($0.80 \leqslant x \leqslant 2.00$) to have low activities, while the activities of Ni-rich catalysts increased dramatically with increased Ni content ($0.03 \leqslant x \leqslant 0.60$). The highest HDS activity was measured for a catalyst having a nominal precursor composition of $Fe_{0.03}Ni_{1.97}P_{2.00}/SiO_2$; this catalyst was 40% more active than a optimized nickel phosphide catalyst prepared from a precursor having a nominal composition of $Ni_{2.00}P_{1.60}/SiO_2$. The 25 wt.% $Fe_{0.03}Ni_{1.97}P_{2.00}/SiO_2$ catalyst also had a dibenzothiophene HDS activity just over 10% higher than that of the 25 wt.% $Ni_{2.00}P_{1.60}/SiO_2$ catalyst at 548 K. The trend of increasing HDS activity for the $Fe_xNi_{2-x}P_y/SiO_2$ catalysts correlates with preferential Fe occupation of M(1) sites (and, therefore, Ni occupation of M(2) sites). Supported by X-ray photoelectron spectroscopy and oxygen chemisorption measurements, we conclude that the high activity of Ni-rich $Fe_xNi_{2-x}P_y/SiO_2$ catalysts can be traced to a high surface density of Ni in M(2) sites that are resistant to site blockage due to S incorporation.

1. Introduction

A substantial body of literature has shown that metal phosphide catalysts have promising properties for the removal of sulfur and nitrogen impurities present in fossil fuels [1]. Recent investigations of metal phosphide catalysts have shown that the hydrotreating properties of monometallic phosphides can be improved by the incorporation of a second metal to form bimetallic phosphides [2–4]. Abu and Smith [2] reported an unsupported $Co_{0.08}Ni_2P$ catalyst to have an activity 67% higher than that of a Ni_2P catalyst for hydrodesulfurization (HDS) of 4,6-dimethyldibenzothiophene (4,6-DMDBT), while Burns et al. [4] observed a $Co_{0.08}Ni_{1.92}P_{2.00}/SiO_2$ catalyst to be 34% higher than that of an $Ni_{2.00}P_{1.60}/SiO_2$ catalyst for thiophene HDS. In addition to having higher HDS activities in some cases, bimetallic phosphide catalysts have exhibited selectivities different than monometallic phosphides [2], indicating that the catalytic properties can be tailored by altering the composition of phosphide catalysts. The higher HDS activities and altered selectivities of the bimetallic phosphide catalysts were attributed to surface enrichment of the catalysts in phosphorus. Burns et al. [4] observed surface P enrichment for a highly active $Co_{0.08}Ni_{1.92}P_{2.00}/SiO_2$ catalyst, while an optimized $Ni_{2.00}P_{1.60}/SiO_2$ catalyst had a Ni-rich surface; the bimetallic phosphide catalyst incorporated less S and had a higher chemisorption capacity after treatment in H_2S/H_2 than did the nickel phosphide catalyst. The higher thiophene HDS activity of the $Co_{0.08}Ni_{1.92}P_{2.00}/SiO_2$ catalyst was attributed to P-enriched surfaces that were resistant to site blockage due to S incorporation during HDS. Abu and Smith [2] concluded that surface P enrichment of an unsupported $Co_{0.08}Ni_2P$ catalyst resulted in surface acid sites that promoted isomerization of the methyl groups of 4,6-DMDBT to give methyl-substituted DBTs that more readily underwent HDS by the DDS pathway.

* Corresponding author at: Department of Chemistry, MS-9150, Western Washington University, 516 High Street, Bellingham, WA 98225, United States. Fax: +1 360 650 2826.
E-mail address: Mark.Bussell@wwu.edu (M.E. Bussell).

0021-9517/$ - see front matter © 2010 Elsevier Inc. All rights reserved.
doi:10.1016/j.jcat.2010.03.016

The goal of the current study was to probe the relationship between the solid-state and surface chemistry of a series of bimetallic phosphide catalysts having a range of compositions and the HDS properties of these catalysts. For this purpose, unsupported and silica-supported $Fe_xNi_{2-x}P$ materials were selected for this study as this bimetallic phosphide system exhibits complete solid-phase miscibility, and the presence of Fe in the materials permits the use of Mossbauer spectroscopy to probe the solid-state chemistry of the catalysts [5,6]. Specifically, the preferential ordering of Fe in the tetrahedral and pyramidal sites in the hexagonal crystal structure was determined, and the results correlated with the surface composition, chemisorption properties, and HDS activities and selectivities of the $Fe_xNi_{2-x}P/SiO_2$ catalysts.

2. Experimental methods

2.1. Catalyst synthesis

Unsupported $Fe_xNi_{2-x}P$ materials were prepared with metal compositions corresponding to x values in the range $0.01 \leqslant x \leqslant 2.00$. In all cases, the phosphorus-to-metal molar ratio (P/Me) of the precursors was P/Me = 1.0. As an example, unsupported $Fe_{1.00}Ni_{1.00}P$ was prepared as follows. A solution composed of 1.3874 g (3.43 mmol) $Fe(NO_3)_3{\cdot}9H_2O$ (Fisher Scientific, ACS Grade) and 0.9983 g (3.43 mmol) $Ni(NO_3)_2{\cdot}6H_2O$ (Alfa Aesar, 99.9985%) dissolved in 10-mL nanopure water was combined with a solution of 0.4538 g (3.44 mmol) $(NH_4)_2HPO_4$ (Alfa Aesar, ACS Grade) dissolved in 5-mL nanopure water and, after mixing, the solution was evaporated to dryness at 383 K. The resulting solid was ground and calcined in air at 773 K for 3 h, and then reduced in a 300 mL/min H_2 (Airgas, 99.999%) while the temperature was increased from room temperature to 923 K at a rate of 1 K/min. Following cooling to room temperature in continued H_2 flow, the unsupported $Fe_{1.00}Ni_{1.00}P$ was subjected to a 60 mL/min He flow for 30 min followed by passivation in a 1.0 mol% O_2/He (Airgas) mixture at 30 mL/min for 2 h.

Oxidic precursors of $Fe_xNi_{2-x}P_y/SiO_2$ catalysts (with metal loadings equivalent to 25 wt.% Me_2P, Me = Fe + Ni) were prepared as follows. Prior to use, the silica support (SiO_2, Cab-O-Sil, M-7D grade, 200 m^2/g) was calcined in air at 773 K for 3 h. The silica was then impregnated with an aqueous solution of $Fe(NO_3)_2{\cdot}9H_2O$ and $Ni(NO_3)_2{\cdot}6H_2O$ followed by drying at 383 K. The dried material was subsequently impregnated with $NH_4H_2PO_4$, followed by drying at 383 K, and calcination at 773 K for 3 h. The synthesis of a $Fe_{1.00}Ni_{1.00}P_{1.20}/SiO_2$ catalyst is described as an example. A solution of 0.4740 g (4.12 mmol) $NH_4H_2PO_4$ (Baker, 99.1%) dissolved in ~10 mL nanopure water was added to a solution of 1.3898 g (3.44 mmol) $Fe(NO_3)_3{\cdot}9H_2O$ and 1.0006 g (3.45 mmol) $Ni(NO_3)_2{\cdot}6H_2O$ dissolved in ~20 mL nanopure water. This solution was then transferred to 1.50 g SiO_2 via multiple impregnations to incipient wetness. After each impregnation, the sample was dried at 383 K for approximately 1 h and was then dried an additional 24 h after the final impregnation. The dried precursor of the $Fe_{1.00}Ni_{1.20}P_{1.20}/SiO_2$ catalyst was calcined, reduced, and passivated as described above for the unsupported $Fe_{1.00}Ni_{1.00}P$. The naming scheme adopted in this study is based on the nominal compositions of the oxidic precursors of the catalysts (e.g. $Fe_{1.00}Ni_{1.00}P_{1.20}/SiO_2$), and does not reflect the actual chemical compositions of the phosphide catalysts.

2.2. Catalyst characterization

2.2.1. Bulk characterization measurements

X-ray diffraction (XRD) patterns of the $Fe_xNi_{2-x}P_y/SiO_2$ catalysts were obtained using a PANalytical X'Pert Pro diffractometer equipped with a monochromatic Cu Kα source (λ = 1.54050 Å). Approximately 0.020 g of catalyst was mixed with a small amount of acetone and the mixture deposited onto a microscope slide. Following evaporation of the acetone, the microscope slide was mounted on the sample stage for XRD pattern acquisition. Mössbauer spectra were recorded at room temperature with a constant-acceleration spectrometer (Wissel GMBH, Germany) in a horizontal transmission mode using a 50 mCi ^{57}Co source. Approximately 0.030 g of unsupported $Fe_xNi_{2-x}P$ or of a $Fe_xNi_{2-x}P_y/SiO_2$ catalyst was loaded into the sample cell for each measurement. Data acquisition varied from 2 h to 5 days depending on the iron content of the sample. The velocity scale was normalized with respect to metallic iron at room temperature; hence all isomer shifts were recorded relative to metallic iron. The Mössbauer spectra were fitted by assuming Lorentzian line shapes using the NORMOS (Wissel GMBH) least-square fitting program. In fitting the spectra, quadrupole spectral components corresponding to the two different sites of iron (M(1) and M(2) sites) in the unsupported and silica-supported $Fe_xNi_{2-x}P$ materials were assumed and the theoretical fit to the experimental data is the sum of these two sub-spectra. The isomer shifts, quadrupole splittings, peak line widths and peak areas were determined from the fitted sub-spectra. The fractional occupation of M(1) and M(2) sites by Fe in the unsupported and silica-supported $Fe_xNi_{2-x}P$ materials was determined from the peak areas of the sub-spectra.

2.2.2. Surface characterization measurements

X-ray photoelectron spectroscopy (XPS) measurements were carried out using a Physical Electronics Quantum 2000 Scanning ESCA Microprobe system with a focused monochromatic Al Kα X-ray (1486.7 eV) source and a spherical section analyzer. The XPS measurements were carried out for as-prepared and HDS-tested $Fe_xNi_{2-x}P_y/SiO_2$ catalysts following passivation and transfer through air to the spectrometer. The spectra were collected with a pass energy of 23.5 eV. The spectra were referenced to an energy scale with binding energies for Cu($2p_{3/2}$) at 932.67 ± 0.05 eV and Au(4f) 84.0 ± 0.05 eV. Low-energy electrons and argon ions were used for specimen neutralization. Binding energies were corrected for sample charging using the C(1s) peak at 284.6 eV for adventitious carbon as a reference. Due to overlap of the Ni $L_3M_{23}M_{48}$ Auger line (706 eV binding energy) with the Fe($2p_{3/2}$) region, Fe surface concentrations were estimated following subtraction of the Ni Auger line contribution to the Fe($2p_{3/2}$) peak area.

BET surface area measurements were acquired using a Micromeritics PulseChemisorb 2700 instrument. In a quartz sample tube, 0.1000 g of catalyst was placed and degassed at room temperature in a 60 mL/min He flow for 30 min. The sample was treated in a flow of He (45 mL/min) for 2 h at 623 K and then cooled to room temperature in a continued He flow. The BET measurements were carried out as described elsewhere [7].

Oxygen (O_2)-pulsed chemisorption measurements were also obtained using the Micromeritics PulseChemisorb 2700 instrument. A 0.1000 g of catalyst was degassed in 60 mL/min He at room temperature for 30 min. Prior to the measurements, the samples were either reduced or sulfided in situ. For reduction, samples were heated from room temperature to 650 K in a 60 mL/min flow of H_2 and held at this temperature for 2 h. For sulfidation, samples were heated from room temperature to 650 K in a 60 mL/min flow of a 3.0 mol% H_2S/H_2 mixture, held at this temperature for 2 h, and then reduced in a 60 mL/min flow of H_2 at 623 K for 1 h. All of the samples were then degassed in 45 mL/min He at 673 K for 1 h. The O_2 chemisorption capacity measurements were carried out at 196 K using a procedure described elsewhere [7]. A 10.3 mol% O_2/He mixture (Airco) was used to obtain the O_2 chemisorption capacity measurements.

2.3. HDS activity measurements

Thiophene HDS activity measurements were carried out using an atmospheric pressure flow reactor according to a method described previously [7,8]. All catalysts were degassed in He (60 mL/min) at room temperature for 30 min. The sample was then heated to the reaction temperature of 643 K, and the flow was switched to a 3.2 mol% thiophene/H_2 reactor feed (50 mL/min). The gas effluent was sampled at 1 h intervals and the final measurement was taken after 48-h on-stream. The total product peak areas from the chromatogram were used to calculate the thiophene HDS activities (nmol Th/g cat s) for the catalysts.

Dibenzothiophene (DBT) HDS activity measurements were carried out using a fixed-bed flow reactor operating at a total pressure of 3.0 MPa and temperatures in the range 498–573 K. The reactor feed consisted of a decalin solution containing 3000 ppm dibenzothiophene and 500 ppm dodecane, with the latter serving as an internal standard for gas chromatographic analysis of the reactor effluent. The liquid feed (5 mL/h) was injected into a 100 mL/min flow of hydrogen and vaporized prior to entry into the reactor. Approximately 0.15 g of catalyst (16–20 mesh size) was diluted with quartz sand to a total volume of 5 mL and loaded into a reactor tube having a diameter of 1.1 cm and length of 40 cm. The weight hourly space velocity (WHSV) was 33 h^{-1}. The reactor temperature was measured with a thermocouple mounted axially in the reactor tube that was in direct contact wit the catalyst bed. With the catalyst at room temperature, the reactor was flushed with 60 mL/min He for 30 min and then pressurized to 3.0 MPa with H_2. The He (Airgas, 99.999 mol%) and H_2 (Airgas, 99.999 mol%) were passed through molecular sieve and O_2 removal traps prior to use. Following pressurization of the reactor with H_2, the catalyst was heated to 498 K in a 150 mL/min flow of H_2 over 30 min after which the flow of liquid feed was begun. The reactor was stabilized for approximately 12 h prior to sampling the reactor effluent at 3-h intervals over 12 h. The catalyst temperature was then raised 25 K, the reactor stabilized for 12 h, followed by sampling of the reactor effluent at 3-h intervals. This procedure was repeated until sampling at the maximum catalyst temperature (573 K) was completed. The samples of the reactor effluent were analyzed off-line using a gas chromatograph (Agilent 6890N) equipped with an HP-5 column and a flame ionization detector.

Prior to the DBT HDS measurement for the commercial Co–Mo/Al_2O_3 catalyst, a 0.15 g sample of the catalyst was subjected to a sulfidation pretreatment in which it was heated from room temperature to 650 K in 1 h in a 60 mL/min flow of a 3.0 mol% H_2S/H_2 mixture and then held at this temperature for 2 h. Following cooling to room temperature, the reactor was pressurized with H_2 and the DBT HDS measurement carried out as described above.

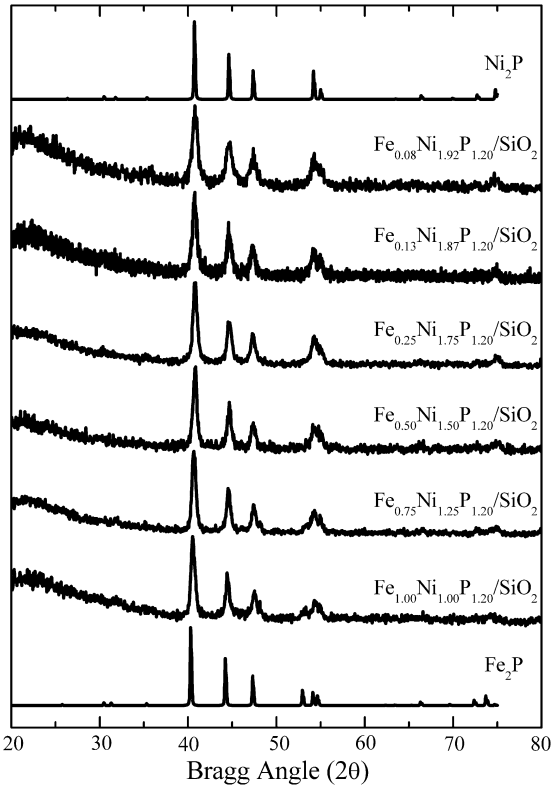

Fig. 1. XRD patterns for $Fe_xNi_{2-x}P_{1.20}/SiO_2$ catalysts having different metal ratios.

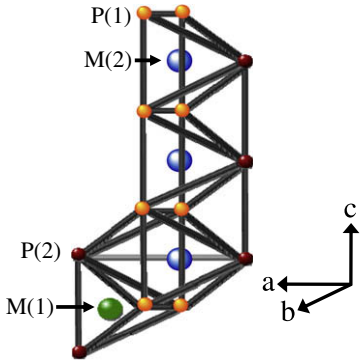

Fig. 2. M_2P structure (M = Fe, Ni) showing the tetrahedral M(1) and pyramidal M(2) sites. Adapted from Ref. [19].

3. Results

3.1. Bulk characterization of $Fe_xNi_{2-x}P_{1.20}/SiO_2$ catalysts

X-ray diffraction patterns for $Fe_xNi_{2-x}P_{1.20}/SiO_2$ catalysts with a range of metal compositions are shown in Fig. 1, while XRD patterns for the unsupported $Fe_xNi_{2-x}P$ materials can be found in Supplementary material (Fig. S1). The XRD patterns for the bimetallic phosphide phases are consistent with the JCPDS reference patterns for Fe_2P (card no. 089-3680 [9]) and Ni_2P (card no. 089-2742 [9]). There are subtle differences in the reference patterns for Fe_2P and Ni_2P, which share the same hexagonal crystal structure ($P\bar{6}2$ m space group). The (0 0 2) reflection at 52.9° is observed for Fe_2P, but not for Ni_2P; the (1 1 1) reflection is located at 40.3° for Fe_2P and at 40.7° for Ni_2P. The $Fe_{1.00}Ni_{1.00}P_{1.20}/SiO_2$ catalyst exhibits the (0 0 2) reflection associated with Fe_2P, but the more Ni-rich $Fe_xNi_{2-x}P_{1.20}/SiO_2$ catalysts do not show this reflection. The (1 1 1) reflection is observed at 40.5° for the $Fe_{1.00}Ni_{1.00}P_{1.20}/SiO_2$ catalyst, but gradually shifts with increasing Ni content to 40.9° for the $Fe_{0.25}Ni_{1.75}P_{1.20}/SiO_2$ catalyst. Further increase in the Ni content results in a slight shift of the (1 1 1) reflection to 40.8° for the $Fe_{0.13}Ni_{1.87}P_{1.20}/SiO_2$ and $Fe_{0.03}Ni_{1.97}P_{1.20}/SiO_2$ catalysts, which is close to the position of this reflection observed for Ni_2P. These observations are consistent with the results of Fruchart et al. [5], which showed that $Fe_xNi_{2-x}P$ solid solutions do not obey Vegard's Law. A minimum in the unit cell volume was observed for a composition of $Fe_{0.30}Ni_{1.70}P$, which is close to the composition ($Fe_{0.25}Ni_{1.75}P_{1.20}/SiO_2$) at which we observed the highest Bragg angle for the (1 1 1) reflection. Based on calculations using the Scherrer equation using the full-width at half maximum for the (1 1 1) reflection, the $Fe_xNi_{2-x}P_{1.20}/SiO_2$ catalysts had crystallite sizes in the 17–23 nm range with an average of 20 nm. The XRD pattern for a $Fe_{0.03}Ni_{1.97}P_{2.00}/SiO_2$ catalyst is shown in Fig. 8; this pattern as well as

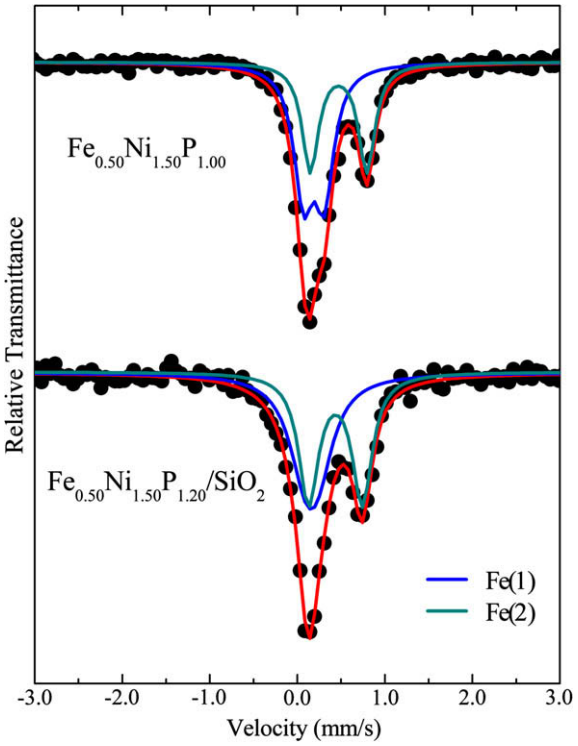

Fig. 3. Mössbauer spectra of unsupported $Fe_{0.50}Ni_{1.5}P$ and a 25 wt.% $Fe_{0.50}Ni_{1.50}P_{1.20}/SiO_2$ catalyst.

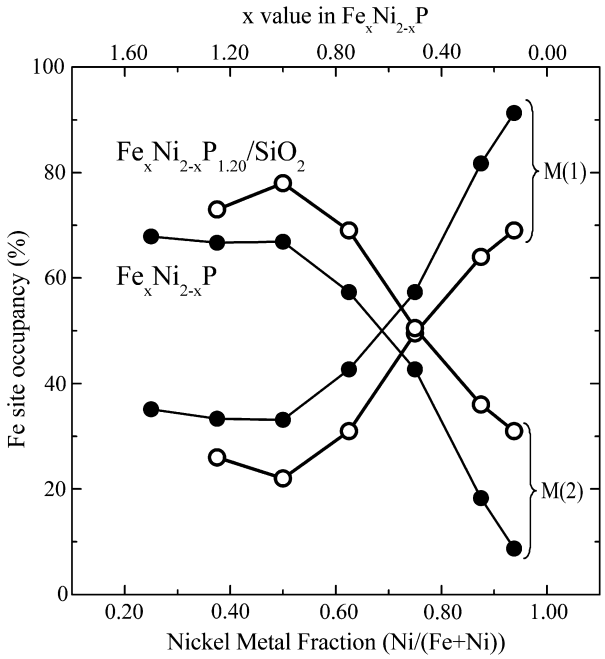

Fig. 4. Plot of iron occupancy of tetrahedral (M(1)) and pyramidal (M(2) sites of unsupported $Fe_xNi_{2-x}P$ materials and $Fe_xNi_{2-x}P_{1.20}/SiO_2$ catalysts as a function of the Ni metal fraction.

those for the other $Fe_{0.03}Ni_{1.97}P_y/SiO_2$ catalysts containing additional excess P in the oxidic precursors ($1.2 < y \leqslant 2.2$) are similar to those shown in Fig. 1 for the $Fe_xNi_{2-x}P_{1.20}/SiO_2$ catalysts. The average crystallite size calculated for the $Fe_{0.03}Ni_{1.97}P_{2.00}/SiO_2$ catalyst was 16 nm.

The Mössbauer spectra acquired for unsupported $Fe_xNi_{2-x}P$ materials were similar to those reported in the literature. Shown in Fig. 3 are Mössbauer spectra for $Fe_{0.50}Ni_{1.50}P$ and a 25 wt.% $Fe_{0.50}Ni_{1.50}P_{1.20}/SiO_2$ catalyst. In addition to the raw spectral data (solid circles), the fitted spectral components for Fe in M(1) and M(2) sites and the overall fitted spectrum are shown (solid lines). For $Fe_{0.50}Ni_{1.50}P$, a central isomer shift (CS) and quadrupole splitting (QS) of 0.20 and 0.21 mm/s were measured, respectively, for Fe in the M(1) site. A CS of 0.47 mm/s and a QS of 0.65 mm/s were measured for Fe in the M(2) site. These Mössbauer spectral values are consistent with those reported for Fe_2P [10] and $Fe_{1.86}Ni_{0.14}P$ [11]. The Mössbauer spectrum for the 25 wt.% $Fe_{0.50}Ni_{1.50}P_{1.20}/SiO_2$ catalyst was similar to that of the unsupported $Fe_{0.50}Ni_{1.50}P$, but with some notable differences. The spectral components fitted for Fe in M(1) and M(2) sites were broadened and, due to this broadening, the quadrupole splitting for Fe in M(1) sites was no longer apparent. The CS for the M(1) spectral component was 0.16 mm/s and the CS and QS for the M(2) spectral component were 0.47 and 0.60 mm/s, respectively. The full-width at half maximum for a peak in the M(2) doublet increased from 0.18 mm/s for unsupported $Fe_{0.50}Ni_{1.50}P$ to 0.30 mm/s for the 25 wt.% $Fe_{0.50}Ni_{1.50}P_{1.20}/SiO_2$ catalyst. The relative peak areas for the M(1) and M(2) spectral components were different for the unsupported and silica-supported materials, with the 25 wt.% $Fe_{0.50}Ni_{1.50}P_{1.20}/SiO_2$ catalyst having a larger M(2) spectral peak area (relative to the M(1) peak area) than for the unsupported $Fe_{0.50}Ni_{1.50}P$. This indicates that more Fe resides in M(2) sites in the 25 wt.% $Fe_{0.50}Ni_{1.50}P_{1.20}/SiO_2$ catalyst than in unsupported $Fe_{0.50}Ni_{1.50}P$. For the $Fe_{0.50}Ni_{1.50}P_{1.20}/SiO_2$ catalyst, 49% of the Fe resides in M(1) sites and 51% in M(2) sites, while for the unsupported $Fe_{0.50}Ni_{1.50}P$, 57% of the Fe resides in M(1) sites and 43% in M(2) sites.

Shown in Fig. 4 are the relative Fe site occupancies for samples of unsupported $Fe_xNi_{2-x}P$ and 25 wt.% $Fe_xNi_{2-x}P_{1.20}/SiO_2$ catalysts plotted as a function of the Ni metal fraction in the samples. The trend of relative site occupancies for the unsupported $Fe_xNi_{2-x}P$ as a function of metal composition is consistent with that observed by Maeda and Takashima [12]; relative site occupancies can be calculated from the Fe site occupancy numbers reported in that study. For the unsupported $Fe_xNi_{2-x}P$, Fe preferentially resides in M(2) sites for $x > \sim 0.60$, but this site preference is reversed for the Ni-rich materials. For $Fe_{0.13}Ni_{1.87}P$, the most Ni-rich material analyzed by Mössbauer spectroscopy, 91% of Fe atoms were observed to reside in M(1) sites and 9% in M(2) sites. Noting the metal composition of this sample, it follows that 47% of the Ni resides in M(1) sites and 53% resides in (M2) sites. For the 25 wt.% $Fe_{0.13}Ni_{1.87}P_{1.20}/SiO_2$ catalyst, 69% of the Fe atoms were determined to reside in M(1) sites and 31% to reside in M(2) sites. From the Fe site occupations, it can be shown that 49% of Ni atoms reside in M(1) sites and 51% in M(2) sites for this catalyst.

3.2. Surface characterization of $Fe_xNi_{2-x}P_{1.20}/SiO_2$ catalysts

XPS spectra in the Ni($2p_{3/2}$) and P($2p_{3/2}$) regions for the $Fe_xNi_{2-x}P_y/SiO_2$ catalysts were similar to those reported previously for $Co_xNi_{2-x}P_y/SiO_2$ catalysts [4]. Due to the overlap of the Ni $L_3M_{23}M_{48}$ Auger emission at 706 eV (on the binding energy scale) with the Fe($2p_{3/2}$) region, binding energies were not determined for Fe. XPS spectra for a representative catalyst, $Fe_{0.25}Ni_{1.75}P_{1.20}/SiO_2$, are shown in Supplementary material (Fig. S2). Since the $Fe_xNi_{2-x}P_y/SiO_2$ catalysts were passivated in a 1 mol% O_2/He mixture following TPR synthesis, the XPS spectra in Ni($2p_{3/2}$) and P($2p_{3/2}$) regions show peaks for oxidized species as well as for underlying reduced species associated with the phosphide phase. The binding energies for the oxidized Ni (856.5–856.8 eV) and P (~133.5 eV) are consistent with assignments to $Ni^{2+}$and P^{5+} species, respectively [4,13]. The binding energies for peaks associated with reduced Ni (853.0–853.3 eV) species are just above those re-

Table 1
Nominal and surface compositions of $Fe_xNi_{2-x}P/SiO_2$ catalysts.

Catalyst	Nominal composition normalized to P	Surface composition (as-prepared)	Surface composition (post-HDS)
$Fe_{2.00}P_{1.00}$	$Fe_{2.00}P_{1.00}$	$Fe_{4.00}P_{1.00}$	$Fe_{3.37}P_{1.00}S_{0.30}$
$Fe_{0.25}Ni_{1.75}P_{1.20}$	$Fe_{0.21}Ni_{1.46}P_{1.00}$	$Fe_{0.14}Ni_{1.64}P_{1.00}$	$Fe_{0.23}Ni_{1.89}P_{1.00}S_{0.18}$
$Fe_{0.13}Ni_{1.87}P_{1.20}$	$Fe_{0.11}Ni_{1.56}P_{1.00}$	$Fe_{0.08}Ni_{1.52}P_{1.00}$	$Fe_{0.03}Ni_{1.16}P_{1.00}S_{0.06}$
$Fe_{0.08}Ni_{1.92}P_{1.20}$	$Fe_{0.07}Ni_{1.60}P_{1.00}$	$Fe_{0.06}Ni_{1.14}P_{1.00}$	$Fe_{0.04}Ni_{1.54}P_{1.00}S_{0.09}$
$Fe_{0.03}Ni_{1.97}P_{2.000}$	$Fe_{0.02}Ni_{0.99}P_{1.000}$	$Fe_{0.05}Ni_{1.63}P_{1.00}$	$Fe_{0.12}Ni_{1.49}P_{1.00}S_{\leqslant 0.05}$
$Ni_{2.00}P_{1.60}$	$Ni_{1.25}P_{1.00}$	$Ni_{2.23}P_{1.00}$	$Ni_{2.87}P_{1.00}S_{0.32}$

ported for zero-valent Ni (852.5–852.9 eV [14]), while the binding energies for reduced P species (129.6–130.0 eV) are slightly below that of elemental phosphorus (130.2 eV [14]). Mar and coworkers recently reported XPS results for unsupported bimetallic phosphides of nickel, including for $Fe_xNi_{2-x}P$ materials having $x = 0.4$, 1.0, and 1.6 [15]. The samples, which were prepared from the elements at high temperatures, were sputter-cleaned in vacuum to remove oxidized surface species prior to XPS spectral acquisition. Small shifts of the Ni($2p_{3/2}$)- and P(2p)-binding energies were observed depending on the composition of the $Fe_xNi_{2-x}P$ materials. The Ni($2p_{3/2}$)-binding energy shifted from 852.89 eV for Ni_2P to 853.07 eV for $Fe_{1.6}Ni_{0.4}P$. The most Ni-rich sample, $Fe_{0.4}Ni_{1.6}P$, had a binding energy of 852.87 eV that was just below that of Ni_2P. A weak dependence of the binding energy on composition was also observed in the P(2p) region. The $Fe_xNi_{2-x}P$ samples had P(2p)-binding energies in the range 129.36–129.44, which fall between the values measured for Fe_2P (129.31 eV) and Ni_2P (129.45 eV) [15]. The somewhat higher Ni($2p_{3/2}$)- and P($2p_{3/2}$)-binding energies observed for the $Fe_xNi_{2-x}P_y/SiO_2$ catalysts may be due to the nature of the samples, nanometer-sized particles supported on silica, or the presence of the passivation layer at the surface of the $Fe_xNi_{2-x}P_y$ particles.

Surface compositions determined for a few as-prepared and HDS-tested $Fe_xNi_{2-x}P_y/SiO_2$ catalysts are listed in Table 1. The monometallic phosphide catalysts $Fe_{2.00}P_{1.00}/SiO_2$ and $Ni_{2.00}P_{1.60}/SiO_2$, which correspond to phase-pure Fe_2P and Ni_2P on the silica support, respectively, both had metal-rich surface compositions ($P^s/Me^s < 0.50$) relative to the expected molar ratio (P/Me = 0.50) from the stoichiometry of the bulk materials. The bimetallic phosphide catalysts had P-rich surfaces ($P^s/Me^s > 0.50$) compared to the expected bulk molar ratios. The $Fe_xNi_{2-x}P_y/SiO_2$ catalysts listed in Table 1, which are Ni-rich materials, had surface compositions that lie in the range $0.56 \leqslant P^s/Me^s \leqslant 0.83$. We reported similar results for Ni-rich $Co_xNi_{2-x}P_y/SiO_2$ catalysts [4] as did Abu and Smith for unsupported Co_xNi_2P catalysts [2].

The BET surface areas and oxygen (O_2) chemisorption capacities of the $Fe_xNi_{2-x}P_y/SiO_2$ catalysts are listed in Table 2. The surface areas of the catalysts were similar, while the O_2 chemisorption capacities varied depending on the metal content of the catalysts and the amount of P used in the catalyst precursors. For both H_2 and H_2S/H_2 pretreatments, the chemisorption capacities followed a generally increasing trend as the amount of Ni in the $Fe_xNi_{2-x}P_{1.20}/SiO_2$ catalysts increased. For $Fe_{0.03}Ni_{1.97}P_y/SiO_2$ catalysts, which had different P contents in the oxidic precursors, the O_2 chemisorption values reached maximum values for the $Fe_{0.03}Ni_{1.97}P_{1.20}/SiO_2$ (H_2 pretreatment) and $Fe_{0.03}Ni_{1.97}P_{1.80}/SiO_2$ (H_2S/H_2 pretreatment) catalysts, but then decreased for catalysts with additional P in the precursors. For $Fe_xNi_{2-x}P_{1.20}/SiO_2$ catalysts with high Fe contents ($x \geqslant 0.50$), the O_2 chemisorption capacities following H_2S/H_2 pretreatment were significantly smaller than following a H_2 pretreatment, while for catalysts with high Ni contents, the chemisorption capacities following the two pretreatments were similar or higher for the H_2S/H_2 pretreatment. The O_2 chemisorption capacities recently reported for $Co_xNi_{2-x}P_y/SiO_2$ catalysts are consistent with results for the $Fe_xNi_{2-x}P_y/SiO_2$ catalysts [4].

Table 2
Catalytic data for $Fe_xNi_{2-x}P/SiO_2$ catalysts.

Nominal composition	BET surface area (m^2/g)	Chemisorption capacity ($\mu mol\ O_2/g$)		HDS activity[a] (nmol Th/g s)
		H_2 pretreatment	H_2/H_2S pretreatment	
$Fe_{2.00}P_{1.00}$	110	42	49	47
$Fe_{1.25}Ni_{0.75}P_{1.10}$	107	44	35	385
$Fe_{1.00}Ni_{1.00}P_{1.10}$	100	50	23	467
$Fe_{0.75}Ni_{1.25}P_{1.20}$	121	53	36	423
$Fe_{0.50}Ni_{1.50}P_{1.20}$	107	104	34	1050
$Fe_{0.25}Ni_{1.75}P_{1.20}$	110	173	143	1070
$Fe_{0.13}Ni_{1.87}P_{1.20}$	97	128	172	1650
$Fe_{0.08}Ni_{1.92}P_{1.20}$	124	118	215	2200
$Fe_{0.03}Ni_{1.97}P_{1.20}$	89	200	125	2540
$Fe_{0.03}Ni_{1.97}P_{1.40}$	109	157	141	2360
$Fe_{0.03}Ni_{1.97}P_{1.60}$	100	131	215	2710
$Fe_{0.03}Ni_{1.97}P_{1.80}$	94	172	274	3230
$Fe_{0.03}Ni_{1.97}P_{2.000}$	112	170	163	3210
$Ni_{2.00}P_{1.60}$	81	153	135	2280

[a] Thiophene HDS activity after 48-h on-stream.

3.3. HDS activities of $Fe_xNi_{2-x}P_y/SiO_2$ catalysts

The thiophene HDS activities of the $Fe_xNi_{2-x}P_y/SiO_2$ catalysts (after 48-h on-stream) are listed in Table 2 and are plotted as a function of the Ni metal fraction (Ni/(Ni + Fe)) in Fig. 5. Starting from the $Fe_{2.00}P_{1.00}/SiO_2$ catalyst, the HDS activities are low up to and including the $Fe_{0.75}Ni_{1.25}P_{1.20}/SiO_2$ catalyst, but beyond this composition, the activities climb steadily as the catalysts become increasingly Ni-rich. The most Ni-rich $Fe_xNi_{2-x}P_{1.20}/SiO_2$ catalyst tested, $Fe_{0.03}Ni_{1.97}P_{1.20}/SiO_2$, had an activity higher than that of a previously optimized $Ni_{2.00}P_{1.60}/SiO_2$ catalyst [16]. Catalysts having this metal composition, $Fe_{0.03}Ni_{1.97}P_y/SiO_2$, but with larger P excess in the precursors ($1.20 < y \leqslant 2.00$), also had high HDS activities (open circles in Fig. 5). The catalysts having the compositions of $Fe_{0.03}Ni_{1.97}P_{1.80}/SiO_2$ (P/Me = 0.90) and $Fe_{0.03}Ni_{1.97}P_{2.00}/SiO_2$ (P/Me = 1.00) had the highest thiophene HDS activities and were over 40% more active than the optimized $Ni_{2.00}P_{1.60}/SiO_2$ catalyst. Assuming that the O_2 chemisorption capacities following H_2S/H_2 pretreatment provide good estimates of the active site densities under HDS conditions, turnover frequencies (TOFs) of 0.017 and 0.020 s^{-1} can be calculated for the $Ni_{2.00}P_{1.60}/SiO_2$ and $Fe_{0.03}Ni_{1.92}P_{2.00}/SiO_2$ catalysts, respectively. The $Fe_{0.03}Ni_{1.97}P_{2.00}/SiO_2$ catalyst was also slightly more active than a $Co_{0.08}Ni_{1.92}P_{2.00}/SiO_2$ catalyst prepared in our laboratory whose properties are described elsewhere [4]. The $Fe_{0.03}Ni_{1.97}P_{2.00}/SiO_2$ and $Co_{0.08}Ni_{1.92}P_{2.00}/SiO_2$ catalysts had nearly identical thiophene HDS TOFs of 0.020 and 0.019 s^{-1}, respectively.

Dibenzothiophene HDS activity measurements were carried out for the $Fe_{0.03}Ni_{1.97}P_{2.00}/SiO_2$ and $Ni_{2.00}P_{1.60}/SiO_2$ catalysts, and the DBT conversions are plotted as a function of the reaction temperature in Fig. 6. These catalysts were selected for the DBT HDS measurements because their precursor compositions corresponded to the highest thiophene HDS activities for the $Fe_xNi_{2-x}P_y/SiO_2$ and Ni_xP_y/SiO_2 catalysts investigated in this or previous studies [16]. The DBT conversion measured for the 25 wt.% $Ni_{2.00}P_{1.60}/SiO_2$ catalyst at 573 K is similar to that measured by Sun et al. [17] for a 15 wt.% Ni_2P/SiO_2 catalyst at 593 K under similar conditions. These authors calculated a DBT HDS activity of 72.7 nmol DBT/g_{cat} s, which can be compared to the range of 106–133 nmol DBT/g_{cat} s determined for the 25 wt.% $Ni_{2.00}P_{1.60}/SiO_2$ catalyst at 548–573 K. As indicated by the selectivity data plotted in Fig. 7 for DBT HDS at 548 K, the $Ni_{2.00}P_{1.60}/SiO_2$ catalyst exhibited a product selectivity favoring biphenyl (72.5%), indicating that the direct desulfurization (DDS) pathway is the dominant pathway for S removal from the DBT. For these reaction conditions (548 K, 3 MPa), equilibrium strongly favors the formation of bicyclohexane (~100 mol%) [18],

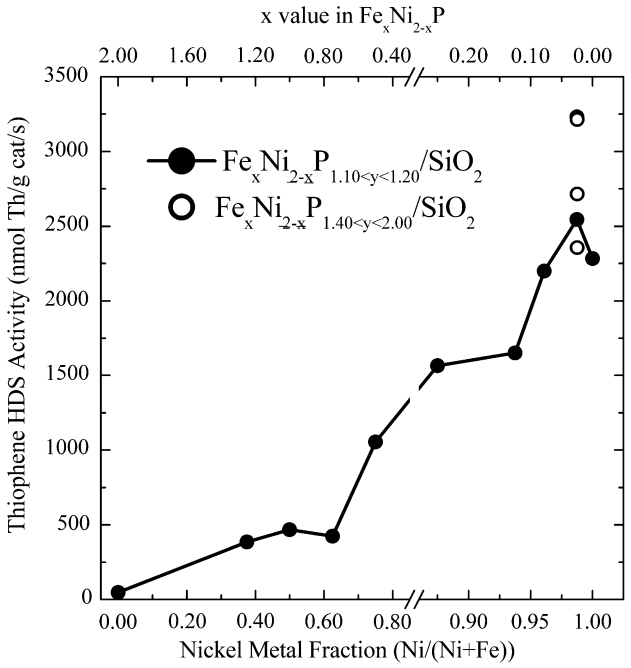

Fig. 5. Thiophene HDS activity versus nominal Ni metal fraction for $Fe_xNi_{2-x}P_y/SiO_2$ catalysts.

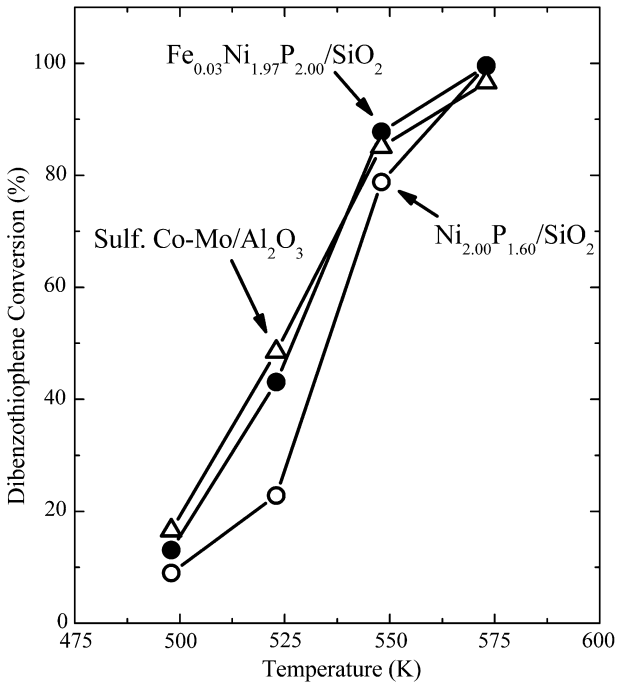

Fig. 6. Dibenzothiophene HDS conversion versus reaction temperature for $Fe_{0.03}Ni_{1.97}P_{2.00}/SiO_2$ and $Ni_{2.00}P_{1.60}/SiO_2$ catalysts.

but this product was not detected in the reactor effluent. The observed selectivity is consistent with that reported by Sun et al. [17] for DBT HDS over Ni_2P/SiO_2 catalysts. Mirroring the thiophene HDS results, the $Fe_{0.03}Ni_{1.97}P_{2.00}/SiO_2$ catalyst is more active than the $Ni_{2.00}P_{1.60}/SiO_2$ catalyst for DBT HDS. At 548–573 K, the $Fe_{0.03}Ni_{1.97}P_{2.00}/SiO_2$ catalyst exhibited higher DBT conversions and had HDS activities of 119–135 nmol DBT/g_{cat} s. The product selectivity for the $Fe_{0.03}Ni_{1.97}P_{2.00}/SiO_2$ catalyst (Fig. 7) shows a preference for biphenyl (67%), but to a lesser extent than was observed for the $Ni_{2.00}P_{1.60}/SiO_2$ catalyst.

Dibenzothiophene HDS TOFs were calculated for the $Fe_{0.03}Ni_{1.97}P_{2.00}/SiO_2$ and $Ni_{2.00}P_{1.60}/SiO_2$ catalysts using their O_2 chemisorption capacities after the H_2S/H_2 pretreatment. Since HDS reaction conditions are those of a sulfiding environment, we believe that the O_2 chemisorption capacities following pretreatment in H_2S/H_2 provide a better estimate of the site densities under reaction conditions than do the chemisorption capacities following pretreatment in H_2. A DBT turnover frequency (TOF) of 7.8×10^{-4} s^{-1} is calculated for the $Ni_{2.00}P_{1.60}/SiO_2$ catalyst at 548 K, while a TOF of 7.3×10^{-4} s^{-1} is calculated for the $Fe_{0.03}Ni_{1.97}P_{2.00}/SiO_2$ catalyst at this same temperature. These TOFs are similar within the error associated with the measurements.

The DBT HDS activities of the 25 wt.% $Ni_{2.00}P_{1.60}/SiO_2$ and $Fe_{0.03}Ni_{1.97}P_{2.00}/SiO_2$ catalysts compare favorably with that of a commercial $Co–Mo/Al_2O_3$ catalyst. At 548–573 K, the $Co–Mo/Al_2O_3$ catalyst had HDS activities in the range 115–131 nmol DBT/g_{cat} s, which are slightly below those measured for the $Fe_{0.03}Ni_{1.97}P_{2.00}/SiO_2$ catalyst. The commercial $Co–Mo/Al_2O_3$ catalyst more strongly favored the DDS reaction pathway, exhibiting a biphenyl selectivity of 91% vs. 67% for the $Fe_{0.03}Ni_{1.97}P_{2.00}/SiO_2$ catalyst. Utilizing the O_2 chemisorption capacity measured for the commercial $Co–Mo/Al_2O_3$ catalyst following pretreatment in H_2S/H_2 (66 μmol O_2/g_{cat}), a DBT TOF of 1.7×10^{-3} s^{-1} is calculated at 548 K. This TOF is twice that of the 25 wt.% $Fe_{0.03}Ni_{1.97}P_{2.00}/SiO_2$ catalyst, but the overall activity of the commercial $Co–Mo/Al_2O_3$ catalyst is lower than that of the phosphide catalyst (on a mass basis) due to its substantially lower site density as measured by O_2 chemisorption.

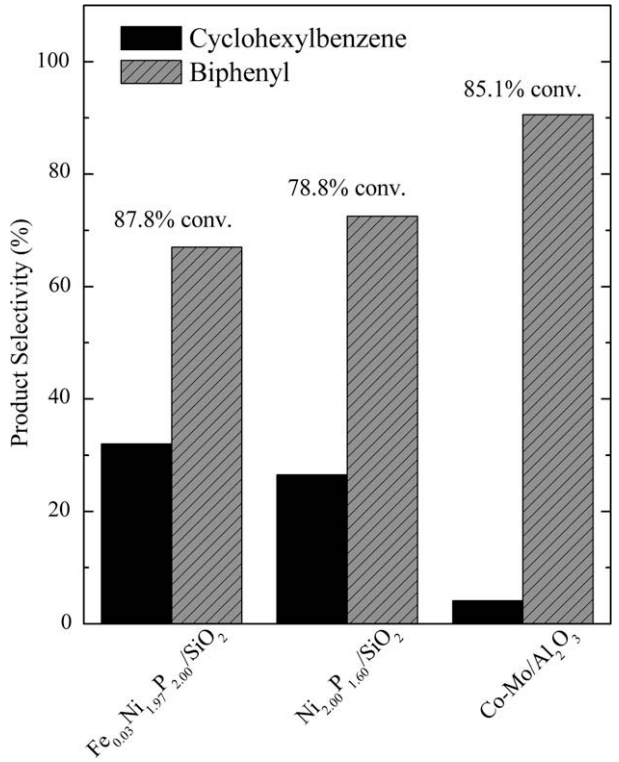

Fig. 7. Dibenzothiophene HDS product selectivity for $Fe_{0.03}Ni_{1.97}P_{2.00}/SiO_2$, $Ni_{2.00}P_{1.60}/SiO_2$ and a commercial $Co–Mo/Al_2O_3$ catalyst for a reaction temperature of 548 K. The DBT HDS conversions at 548 K are given on the figure.

3.4. Characterization of HDS-tested catalysts

XRD patterns and XPS spectra were acquired for selected $Fe_xNi_{2-x}P_y/SiO_2$ catalysts after 48 h of thiophene HDS testing; the surface compositions for these catalysts are listed in Table 1. XRD

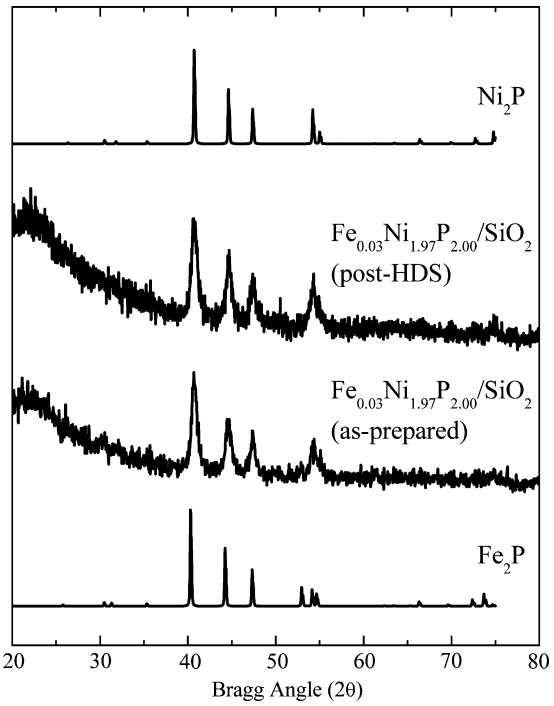

Fig. 8. XRD patterns for as-prepared and thiophene HDS-tested samples of a $Fe_{0.03}Ni_{1.97}P_{2.00}/SiO_2$ catalyst.

patterns of the tested catalysts revealed the loss of phase purity for some of the Ni-rich $Fe_xNi_{2-x}P_{1.20}/SiO_2$ catalysts ($x < 0.50$) as indicated by the presence of XRD peaks associated with $Ni_{12}P_5$. These results are in contrast to those reported previously for $Co_xNi_{2-x}P_{1.00}/SiO_2$ catalysts, for which no loss of phase purity was observed after similar thiophene HDS testing. Shown in Fig. 8 are XRD patterns for as-prepared and HDS-tested samples of a $Fe_{0.03}Ni_{1.97}P_{2.00}/SiO_2$ catalyst. There was no evidence for the loss of phase purity for the HDS-tested catalyst, which is not surprising given the large excess of P used in the catalyst precursor. The average crystallite size calculated for the HDS-tested $Fe_{0.03}Ni_{1.97}P_{2.00}/SiO_2$ catalyst (14 nm) was similar to that calculated for the as-prepared catalyst (16 nm). The surface composition data listed in Table 1 indicate that the bimetallic Fe–Ni phosphide catalysts incorporate less surface S than did the monometallic $Fe_{2.00}P_{1.00}/SiO_2$ and $Ni_{2.00}P_{1.60}/SiO_2$ catalysts during HDS testing. The $Fe_{0.03}Ni_{1.97}P_{2.00}/SiO_2$ catalyst, for example, which had a thiophene HDS activity 40% higher than that of the $Ni_{1.92}P_{1.60}/SiO_2$ catalyst, had a surface S concentration below the XPS detection limit (surface composition: $Fe_{0.12}Ni_{1.49}P_{1.00}S_{\leqslant 0.05}$), while the $Ni_{1.92}P_{1.60}/SiO_2$ catalyst had a surface composition of $Ni_{2.87}P_{1.00}S_{0.32}$. An earlier investigation of $Co_xNi_{2-x}P_y/SiO_2$ catalysts revealed a trend in which the surface S content of HDS-tested catalysts decreased substantially as the surface P content of the as-prepared catalysts increased. The highly active $Co_{0.08}Ni_{1.92}P_{1.60}/SiO_2$ catalyst had the most P-enriched surface and had a post-HDS testing surface composition of $Co_{0.13}Ni_{1.59}P_{1.00}S_{0.06}$, which is similar to that of the HDS-tested $Fe_{0.03}Ni_{1.97}P_{2.00}/SiO_2$ catalyst.

4. Discussion

4.1. Solid-state and surface chemistry of $Fe_xNi_{2-x}P_y/SiO_2$ catalysts

The monometallic phosphides Fe_2P and Ni_2P (and their solid solutions) adopt the same hexagonal structure ($P\bar{6}2m$ space group [19]), in which the metal atoms are either surrounded by four P atoms in a tetrahedral geometry (M(1) site) or by five P atoms in a square pyramidal geometry (M(2) site) [5]. The two kinds of metal (and P) sites for this structure are shown in Fig. 2. The lattice parameters are similar for Fe_2P and Ni_2P with those for Ni_2P being slightly smaller, reflecting the smaller atomic radius for Ni (121 pm [20]) than for Fe (125 pm [20]). The metal–phosphorus distances for Fe_2P and Ni_2P are listed in Table 3; the M–P distances are shorter for metal atoms residing in M(1) sites than in M(2) sites. Electronic structure calculations for Fe_2P and Ni_2P indicate that there is substantial charge density overlap between metal atoms in M(1) sites and neighboring P atoms, and far weaker interaction between metal atoms in M(2) sites and neighboring P atoms [21,22]. Jian-Wang et al. also used electronic structure calculations to probe the effect of substituting Ni atoms for Fe(1) and Fe(2) atoms in Fe_2P [22]. Substitution of Ni into Fe(1) sites led to a small amount of charge transfer from P atoms to the Ni(1) atoms, since Ni is slightly more electronegative than Fe. On the other hand, the electronic structure calculations indicated that substitution of Ni for Fe(2) atoms in Fe_2P resulted in negligible charge transfer. These differences upon Ni substitution into the M(1) and M(2) sites are consistent with the fact that the interaction between metal and P atoms is stronger for the tetrahedral M(1) sites than for the pyramidal M(2) sites.

The XRD patterns for the $Fe_xNi_{2-x}P_y/SiO_2$ catalysts in this study (Figs. 1 and 8) are consistent with the presence of a single metal phosphide phase on the silica support for the full range of composition ($0 \leqslant x \leqslant 2$). $Fe_xNi_{2-x}P$ solid solutions exhibit some unusual properties, and the results obtained in the current study for $Fe_xNi_{2-x}P_y/SiO_2$ catalysts are consistent with those reported previously for the bulk materials. As noted in the Results, $Fe_xNi_{2-x}P$ solid solutions do not obey Vegard's Law, which states that a linear relationship exists between the crystal lattice constant and the concentration of the constituent elements (at constant temperature) [23]. In the case of $Fe_xNi_{2-x}P$ solid solutions, Vegard's law would predict a linear decrease in the lattice parameters with increasing Ni concentration. Instead, Fruchart et al. [5] observed a minimum in the unit cell volume (and the c lattice parameter) for a composition of $Fe_{0.30}Ni_{1.70}P$ followed by an increase in cell volume upon increasing Ni concentration. The XRD results for the $Fe_xNi_{2-x}P_{1.20}/SiO_2$ catalysts are consistent with those for unsupported $Fe_xNi_{2-x}P$ solid solutions; the Bragg angle for the (1 1 1) reflection increases with increasing Ni concentration up to $Fe_{0.25}Ni_{1.75}P_{1.20}/SiO_2$, but then decreases for the more Ni-rich $Fe_xNi_{2-x}P_{1.20}/SiO_2$ catalysts. The non-Vegard Law behavior of $Fe_xNi_{2-x}P$ solid solutions can be understood in terms of the site preferences of the solute metal (e.g. Ni) in the hexagonal lattice of Fe_2P. Energetically, the smaller Ni atoms would be expected to preferentially occupy the more spatially confined M(1) sites in the lattice. As discussed further below, the reverse is observed for Ni-rich $Fe_xNi_{2-x}P$ solid solutions; Ni atoms preferentially occupy M(2) sites for $x \leqslant 0.30$, and an increase in the unit cell volume is observed [5,24]. The XRD results obtained for the $Fe_xNi_{2-x}P_{1.20}/SiO_2$ catalysts are consistent with this behavior.

The ordering of transition metals in a number of bimetallic phosphides, including $Co_xNi_{2-x}P$, $Fe_xNi_{2-x}P$, and $Mn_xNi_{2-x}P$ materials, is well known [5,24]. Mössbauer spectroscopy and neu-

Table 3
Metal–phosphorus distances in Fe_2P and Ni_2P.

Metal phosphide	M(1)–P distance (nm)	M(2)–P distance (nm)	Ref.
Fe_2P	Fe(1)–P(1) 0.2294 Fe(1)–P(2) 0.2215	Fe(2)–P(1) 0.2378 Fe(2)–P(2) 0.2483	[28]
Ni_2P	Ni(1)–P(1) 0.2266 Ni(1)–P(2) 0.2209	Ni(2)–P(1) 0.2369 Ni(2)–P(2) 0.2456	[29]

tron diffraction measurements carried out for $Fe_xNi_{2-x}P$ materials have shown that Fe atoms preferentially occupy M(2) sites over a broad compositional range ($0.3 \leqslant x \leqslant 2.0$), but that Fe preferentially occupies M(1) sites for the Ni-rich materials ($0.0 \leqslant x < 0.3$) [12,25]. For example, neutron diffraction investigation of the Fe-rich material $Fe_{1.50}Ni_{0.50}P$ showed that Fe and Ni were randomly distributed in the M(1) sites, while Fe exclusively occupied the M(2) sites [25]. On the other hand, Mössbauer spectroscopy measurements for the Ni-rich material $Fe_{0.20}Ni_{1.80}P$ revealed Fe and Ni atoms occupied M(2) sites, while Fe atoms exclusively occupied M(1) sites [12]. The Fe site occupancies plotted in Fig. 4, determined from Mössbauer spectra acquired in the current study for unsupported $Fe_xNi_{2-x}P$ materials, are in agreement with the literature findings and show the cross-over of Fe site preference occurring at $x = \sim 0.60$. To our knowledge, Mössbauer spectroscopy had not been used previously to probe the Fe site occupancies in supported $Fe_xNi_{2-x}P$ catalysts. The $Fe_xNi_{2-x}P_{1.20}/SiO_2$ catalysts, prepared with a slight excess of P to achieve phase purity, had average crystallite sizes in the range 17–23 nm, which was substantially smaller than the average crystallite sizes of 45–50 nm for the unsupported $Fe_xNi_{2-x}P$ materials. The Mössbauer spectra of $Fe_{0.50}Ni_{1.50}P$ and a 25 wt.% $Fe_{0.50}Ni_{1.50}P_{1.20}/SiO_2$ catalyst (Fig. 3) are similar, except for line broadening evident in the latter spectrum that is attributed to the smaller particles and/or the influence of the silica support. The plotted Fe site occupancies in Fig. 4 reveal a second difference, altered Fe site preferences for the $Fe_xNi_{2-x}P_y/SiO_2$ catalysts relative to the unsupported materials. The trends in site preferences are similar for the two sets of materials, but are offset from one another with fractionally more Fe residing in M(2) sites for the $Fe_xNi_{2-x}P_y/SiO_2$ catalysts. This offset is most pronounced for the Ni-rich materials. For example, 91% of Fe atoms in $Fe_{0.13}Ni_{1.87}P$ were observed to reside in M(1) sites and 9% in M(2) sites, while for the 25 wt.% $Fe_{0.13}Ni_{1.87}P_{1.20}/SiO_2$ catalyst, 69% of the Fe atoms were determined to reside in M(1) sites and 31% to reside in M(2) sites. Two possible explanations for the higher proportion of Fe in M(2) sites in the supported catalysts relative to the unsupported materials are smaller average crystallite sizes of the $Fe_xNi_{2-x}P_{1.20}/SiO_2$ catalysts (17–23 nm) compared to the unsupported $Fe_xNi_{2-x}P$ materials (45–50 nm) or interactions between the metal phosphide particles and the silica support. If the surfaces of the $Fe_xNi_{2-x}P$ particles are terminated with M(2) sites, which would be consistent with the conclusion of Oyama and Lee for Ni_2P particles [26], then a higher proportion of Fe (and Ni) in M(2) sites would be expected as the surface-to-volume ratio increases with decreased particle size. Mössbauer spectroscopy measurements of catalysts with different particle sizes would be needed to probe this further. The most important finding of the Mössbauer spectroscopy measurements for the Ni-rich $Fe_xNi_{2-x}P_y/SiO_2$ catalysts is that an excess of Ni atoms reside in M(2) sites due to the preferential ordering of the metals in these materials. As discussed above, electronic structure calculations indicate that Ni in M(2) sites of Ni_2P and Ni substituted in M(2) sites of Fe_2P interact weakly with neighboring P atoms, consistent with the Ni being metallic in character.

In a discussion of the structural and magnetic properties of bimetallic phosphides, Goodenough hypothesized that the anomalous site preferences in $Fe_xNi_{2-x}P$ materials can be understood in terms of electron transfer from Fe to Ni in these materials [24]. As mentioned above, the smaller Ni atoms would be expected to preferentially occupy the more spatially confined M(1) sites in the lattice. However, the transfer of electron density from Fe to Ni atoms could explain the preference for Ni atoms to locate in the pyramidal M(2) sites in Ni-rich $Fe_xNi_{2-x}P$ materials. This hypothesis is supported by the recent XPS and X-ray absorption near-edge spectroscopy (XANES) measurements of Mar and coworkers [15]. A slight shift of the Ni($2p_{3/2}$)-binding energy was observed from its value of 852.89 eV for Ni_2P to either higher or lower binding energy depending on the composition of $Fe_xNi_{2-x}P$ materials. For $Fe_{0.4}Ni_{1.6}P$, in which Ni atoms preferentially occupy M(2) sites, the Ni($2p_{3/2}$)-binding energy shifts to a slightly lower binding energy of 852.87 eV. On the other hand, for $Fe_{1.0}Ni_{1.0}P$ and $Fe_{1.6}Ni_{0.4}P$ in which Ni preferentially occupies M(1) sites, the Ni($2p_{3/2}$)-binding energy shifts slightly higher to 853.01 and 853.07 eV, respectively. Further evidence for electron density transfer from Fe to Ni comes from analysis of the satellite intensity in the Ni($2p_{3/2}$) region of the XPS spectra and of the metal XANES spectra [15]. Electron transfer from Fe to Ni would result in an increase in size of the Ni atoms, which could explain why Ni preferentially occupies M(2) sites in the Ni-rich $Fe_xNi_{2-x}P$ materials.

It was not possible to confirm the subtle binding energy shifts observed by Mar and coworkers [15] in our XPS spectra of the $Fe_xNi_{2-x}P_y/SiO_2$ catalysts due to the presence of the passivation layer on the surfaces of the supported bimetallic phosphide particles. The surface compositions listed in Table 1 for $Fe_{2.00}P_{1.00}/SiO_2$, $Ni_{2.00}P_{1.60}/SiO_2$ and a few of the Ni-rich $Fe_xNi_{2-x}P_y/SiO_2$ catalysts are consistent with observations reported previously for $Co_xNi_{2-x}P_y/SiO_2$ catalysts [4]. The Ni-rich bimetallic phosphide catalysts exhibit P-rich surfaces ($P^s/Me^s > 0.50$) relative to the monometallic phosphides, which have metal-rich surfaces ($P^s/Me^s < 0.50$). It is hypothesized that the surface enrichment of P in Ni-rich $Fe_xNi_{2-x}P_y/SiO_2$ and $Co_xNi_{2-x}P_y/SiO_2$ catalysts is associated with an excess of Ni(2) sites at the surfaces of the metal phosphide particles. The Mössbauer spectral results support this hypothesis as the site occupancy results (Fig. 4) show that for $x < \sim 0.60$, Ni atoms preferentially occupy M(2) sites, resulting in an excess of Ni(2) atoms in the Ni-rich $Fe_xNi_{2-x}P_y/SiO_2$ catalysts. Based on extended X-ray absorption fine structure (EXAFS) measurements, Oyama and Lee [26] reported that the distribution of Ni in M(1) and M(2) sites of Ni_2P/SiO_2 catalysts changes as a function of the phosphide particle size. As the Ni_2P crystallite size decreased from 10.1 to 3.8 nm, the proportion of Ni in M(2) sites increased relative to Ni in M(1) sites. The authors concluded that the surfaces of the Ni_2P particles terminate with M(2) sites and, therefore, the proportion of these sites in the particles increases as the particle size decreases. Taken collectively, the EXAFS results for Ni_2P/SiO_2 catalysts [26], the Mössbauer spectroscopy results for $Fe_xNi_{2-x}P_y/SiO_2$ catalysts and the XPS surface compositions for $Fe_xNi_{2-x}P_y/SiO_2$ and $Co_xNi_{2-x}P_y/SiO_2$ catalysts indicate that an excess of Ni(2) atoms are present in the Ni-rich bimetallic phosphide catalysts and that the surfaces of the phosphide particles are enriched in Ni(2) sites.

4.2. HDS properties of $Fe_xNi_{2-x}P_y/SiO_2$ catalysts

The thiophene and dibenzothiophene HDS activities measured for Ni-rich $Fe_xNi_{2-x}P_y/SiO_2$ catalysts are higher than those for an optimized $Ni_{2.00}P_{1.60}/SiO_2$ catalyst. The thiophene HDS results are consistent with those reported previously for $Co_xNi_{2-x}P_y/SiO_2$ catalysts [4]. In particular, a 25 wt.% $Fe_{0.03}Ni_{1.97}P_{2.00}/SiO_2$ catalyst had a thiophene HDS activity that was 40% higher than that of a 25 wt.% $Ni_{2.00}P_{1.60}/SiO_2$ catalyst (at 643 K), and a DBT HDS activity that was 12% higher than that of the nickel phosphide catalyst (at 548 K). Importantly, the 25 wt.% $Fe_{0.03}Ni_{1.97}P_{2.00}/SiO_2$ catalyst was also slightly more active than a commercial $Co–Mo/Al_2O_3$ catalyst for dibenzothiophene HDS in the temperature range 548–573 K. The trend in thiophene HDS activities measured for the $Fe_xNi_{2-x}P_y/SiO_2$ catalysts as a function of Ni metal content (Fig. 5) closely mirrors the trend observed for $Co_xNi_{2-x}P_y/SiO_2$ catalysts [4]. A $Fe_{2.00}P_{1.00}/SiO_2$ catalyst had a very low thiophene HDS activity (as did a $Co_{2.00}P_{1.00}/SiO_2$ catalyst), but the substitution of a small amount of Fe (or Co) into nickel phosphide yielded catalysts (e.g. $Fe_{0.03}Ni_{1.97}P_{2.00}/SiO_2$ and $Co_{0.08}Ni_{1.92}P_{2.00}/SiO_2$) that had

thiophene HDS activities 34–40% higher than that of a $Ni_{2.00}P_{1.60}/SiO_2$ catalyst. These results are consistent with those of Abu and Smith [2], who observed an unsupported $Co_{0.08}Ni_2P$ catalyst to have a significantly higher activity than that of a Ni_2P catalyst for HDS of 4,6-DMDBT.

Based on the HDS activity results summarized above, a number of important conclusions can be made about the properties of bimetallic phosphide catalysts. A key finding is that the positive synergistic effect on HDS activity due to the addition of a second metal to nickel phosphide is not specific to Co, the first metal investigated, but is also observed for Fe and suggests that this effect may be observed for other transition metals as well. The similar thiophene HDS trends observed for the $Fe_xNi_{2-x}P_y/SiO_2$ and $Co_xNi_{2-x}P_y/SiO_2$ catalysts (as a function of Ni metal content) along with the Mössbauer spectroscopy results for the iron-containing catalysts lead us to conclude that high HDS activity correlates with Ni preferential occupation of M(2) sites and enrichment of these pyramidal sites at the surfaces of the metal phosphide particles. $Fe_xNi_{2-x}P$ and $Co_xNi_{2-x}P$ solid solutions exhibit similar Ni site occupancies as a function of metal composition; $Co_xNi_{2-x}P$ solid solutions adopt the hexagonal ($P\bar{6}2$ m space group [19]) over the compositional range for which $0 \leqslant x \leqslant 1.7$ [5]. Neutron diffraction measurements revealed that there is ordering of the metals in the M(1) and M(2) sites in $Co_xNi_{2-x}P$ materials [24,27], similar to what was observed for $Fe_xNi_{2-x}P$ materials in the current and other studies using Mössbauer spectroscopy [12]. Comparison of Fe site occupancy (Fig. 4) and thiophene HDS activity (Fig. 5) plots show that there is a correlation between increasing HDS activity and preferential Fe occupation of M(1) sites (and, therefore, of Ni preferential occupation of M(2) sites) with increasing Ni content of the $Fe_xNi_{2-x}P_y/SiO_2$ catalysts. As described above, Oyama and Lee [26] concluded that the surfaces of the Ni_2P particles in supported catalysts terminate with M(2) sites and, therefore, the proportion of these sites in the particles increases as the particle size decreases. These authors observed that as the proportion of Ni in M(2) sites increases, the bulk P/Ni molar ratio also increases as square pyramidal Ni atoms (M(2)) are surrounded by five P atoms while tetrahedral Ni atoms (M(1)) are surrounded by four P atoms. This finding is consistent with the surface compositions for $Fe_xNi_{2-x}P_y/SiO_2$ (Table 1) and $Co_xNi_{2-x}P_y/SiO_2$ [4] catalysts that show surface enrichment in P for the Ni-rich materials, which have an excess of Ni in M(2) sites. Abu and Smith [2] attributed the high 4,6-DMDBT HDS activity of an unsupported $Co_{0.08}Ni_2P$ catalyst (1.7 times more active for than unsupported Ni_2P) to the enhanced acidity of the bimetallic phosphide catalyst due to its highly P-enriched surface; an excess of surface Ni(2) sites may play a role in the high activity of this catalyst as well.

The DBT product selectivity provides additional insight into the properties of Ni-rich $Fe_xNi_{2-x}P_y/SiO_2$ catalysts that contribute to their higher HDS activity relative to nickel phosphide The 25 wt.% $Fe_{0.03}Ni_{1.97}P_{2.00}/SiO_2$ catalyst showed increased selectivity toward cyclohexylbenzene relative to the 25 wt.% $Ni_{2.00}P_{1.60}/SiO_2$ catalyst (Fig. 7), indicating enhanced HDS via the hydrogenation pathway for the bimetallic phosphide catalyst. Based on structural results from EXAFS measurements and 4,6-DMDBT HDS product selectivities, Oyama and Lee [26] concluded that direct desulfurization occurred on Ni(1) sites of supported Ni_2P particles while HDS via the hydrogenation pathway occurred on Ni(2) sites. This conclusion is consistent with an enrichment of Ni(2) sites at the surface of the bimetallic phosphide particles of the $Fe_{0.03}Ni_{1.97}P_{2.00}/SiO_2$ catalyst, resulting in increased selectivity toward the hydrogenation pathway for this catalyst relative to the $Ni_{2.00}P_{1.60}/SiO_2$ catalyst. Ni-rich $Fe_xNi_{2-x}P_y/SiO_2$ catalysts also have higher site densities (as determined by O_2 chemisorption (Table 2)) and greater resistance to S incorporation under HDS conditions compared to the $Ni_{2.00}P_{1.60}/SiO_2$ catalyst (as determined by XPS, Table 1). We conclude that the improved HDS properties of Ni-rich $Fe_xNi_{2-x}P_y/SiO_2$ catalysts relative to Ni_2P/SiO_2 can be traced to a higher concentration of Ni(2) sites at the surface of the bimetallic phosphide catalysts. It follows, therefore, that the role of Fe in improving the HDS properties of Ni-rich $Fe_xNi_{2-x}P_y/SiO_2$ catalysts is indirect in nature and is related to the preferential ordering of the metals in M(1) and M(2) sites in the crystal structure. A similar conclusion can be drawn for the role of Co in determining the HDS properties of Ni-rich $Co_xNi_{2-x}P_y/SiO_2$ catalysts [4].

5. Conclusions

Investigation of the bulk and surface properties of a series of $Fe_xNi_{2-x}P_y/SiO_2$ catalysts indicates that the high HDS activity of Ni-rich catalysts can be correlated with an excess of Ni(2) sites at the surface of the phosphide particles. Mössbauer spectroscopy measurements revealed ordering of Fe atoms in the $Fe_xNi_{2-x}P_y/SiO_2$ catalysts, with Fe atoms preferentially occupying M(2) sites for catalysts with significant Fe contents ($x > \sim 0.60$), but the Fe site preference reverses to favor M(1) sites as the Fe content decreases ($x < \sim 0.60$). As a consequence, there is an excess of Ni atoms in M(2) sites for the Ni-rich $Fe_xNi_{2-x}P_y/SiO_2$ catalysts. A 25 wt.% $Fe_{0.03}Ni_{1.97}P_{2.00}/SiO_2$ catalyst had a thiophene HDS activity 40% higher than an optimized 25 wt.% $Ni_{2.00}P_{1.60}/SiO_2$ catalyst (at 643 K), and a DBT HDS activity just over 10% higher than that of the nickel phosphide catalyst (at 548 K). The higher HDS activities of Ni-rich $Fe_xNi_{2-x}P_y/SiO_2$ catalysts (relative to $Ni_{2.00}P_{1.60}/SiO_2$) can be traced to higher site densities and greater resistance to S incorporation, which we conclude is due to a higher Ni(2) surface site concentration for the bimetallic catalysts. The trend in HDS activities observed for the $Fe_xNi_{2-x}P_y/SiO_2$ catalysts is similar to that reported previously for $Co_xNi_{2-x}P_y/SiO_2$ catalysts [4] and is consistent with the Ni site preferences, site densities and S resistance also observed for these catalysts. HDS testing using 4,6-DMDBT is warranted to further probe differences in the catalytic properties of supported nickel phosphide and Ni-rich bimetallic phosphide catalysts for deep HDS applications.

Acknowledgments

This research was supported by the National Science Foundation under Grant numbers CHE-0503777 and CHE-0809433. A portion (XPS) of the research described in this paper was performed in the Environmental Molecular Sciences Laboratory (EMSL), a national scientific user facility sponsored by the Department of Energy's Office of Biological and Environmental Research and located at Pacific Northwest National Laboratory.

Appendix A. Supplementary material

Supplementary data associated with this article can be found, in the online version, at doi:10.1016/j.jcat.2010.03.016.

References

[1] S.T. Oyama, T. Gott, H. Zhao, Y.-K. Lee, Catal. Today 143 (2009) 94.
[2] I.I. Abu, K.J. Smith, J. Catal. 241 (2006) 356.
[3] I.I. Abu, K.J. Smith, Appl. Catal. A: Gen. 328 (2007) 58.
[4] A.W. Burns, A.F. Gaudette, M.E. Bussell, J. Catal. 260 (2008) 262.
[5] R. Fruchart, A. Roger, J.P. Senateur, J. Appl. Phys. 40 (1969) 1250.
[6] J.-M.M. Millet, Adv. Catal. 51 (2007) 309.
[7] S.J. Sawhill, D.C. Phillips, M.E. Bussell, J. Catal. 215 (2003) 208.
[8] K.A. Layman, M.E. Bussell, J. Phys. Chem. B 108 (2004) 10930.
[9] JCPDS Powder Diffraction File, International Centre for Diffraction Data, Swarthmore, PA, 2000.
[10] R. Wappling, L. Haggstrom, T. Ericsson, S. Devanarayana, E. Karlsson, B. Carlsson, S. Rundqvist, J. Solid State Chem. 13 (1975) 258.

[11] S. Kumar, A. Krishnamurthy, B.K. Srivastava, Hyperfine Interact. 184 (2008) 155.
[12] Y. Maeda, Y. Takashima, J. Inorg. Nucl. Chem. 35 (1973) 1963.
[13] T. Korányi, Appl. Catal. A: Gen. 239 (2003) 253.
[14] D. Briggs, M.P. Seah (Eds.), Practical Surface Analysis by Auger and X-ray Photoelectron Spectroscopy, John Wiley & Sons, New York, 1983.
[15] P.E.R. Blanchard, A.P. Grosvenor, R.G. Cavell, A. Mar, J. Mater. Chem. 19 (2009) 6015.
[16] S.J. Sawhill, K.A. Layman, D.R. Van Wyk, M.H. Engelhard, C. Wang, M.E. Bussell, J. Catal. 231 (2005) 300.
[17] F. Sun, W. Wu, Z. Wu, J. Guo, Z. Wei, Y. Yang, Z. Jiang, F. Tian, C. Li, J. Catal. 228 (2004) 298.
[18] W.V. Steele, R.D. Chirico, National Institute for Petroleum and Energy Research, vol. 403, NIPER, Bartlesville, OK, 1989, p. 25.
[19] F. Hulliger, Struct. Bond. (Berlin) 4 (1968) 83.
[20] J.E. Huheey, E.A. Keiter, R.L. Keiter, Inorganic Chemistry: Principles of Structure and Reactivity, Harper Collins College Publishers, New York, 1993.
[21] S. Ishida, S. Asano, J. Ishida, J. Phys. F: Met. Phys. 17 (1987) 475.
[22] C. Jian-Wang, L. He-Lie, Z. Qing-Qi, J. Phys.: Condens. Matter 5 (1993) 9307.
[23] A.R. Denton, N.W. Ashcroft, Phys. Rev. A 43 (1991) 3161.
[24] J.B. Goodenough, J. Solid State Chem. 7 (1973) 428.
[25] R. Zach, J. Tobola, B. Sredniawa, S. Kaprzyk, C. Casado, M. Bacmann, D. Fruchart, J. Alloys Compd. 383 (2004) 322.
[26] S.T. Oyama, Y.-K. Lee, J. Catal. 258 (2008) 393.
[27] M. Artigas, M. Bacmann, D. Boursier, D. Fruchart, R. Fruchart, J.L. Soubeyroux, Comptes Rendus de l'Academie des Sciences, Serie II: Mecanique, Physique, Chimie, Sciences de la Terre et de l'Univers, vol. 315, 1992, p. 29.
[28] B. Carlsson, M. Golin, S. Rundqvist, J. Solid State Chem. 8 (1973) 57.
[29] S. Rundqvist, Acta Chem. Scand. 16 (1962) 992.